Optics Letters

Graphene-based meta-coupler for direction-controllable emission of surface plasmons

Hua Zhu,[1] Ming Deng,[1] Shuqi Chen,[2] and Lin Chen[1,*]

[1]Wuhan National Laboratory for Optoelectronics, Huazhong University of Science and Technology, Wuhan 430074, China
[2]Laboratory of Weak Light Nonlinear Photonics Ministry of Education School of Physics, Teda Applied Physics Institute, Nankai University, Tianjin 300071, China
*Corresponding author: chen.lin@mail.hust.edu.cn

Received 15 April 2019; revised 23 May 2019; accepted 9 June 2019; posted 10 June 2019 (Doc. ID 365145); published 1 July 2019

Gradient metasurfaces have offered a promising approach to achieve high-efficiency conversion between surface plasmons (SPs) and propagating waves (PWs), and hence have found numerous applications in photonics. However, the available SP-PW couplers lack flexibility for active control, which limits their use in practice. Graphene-based meta-couplers are proposed to realize dynamical SP-PW conversion by providing a tunable phase shift to the scattering SPs by means of chemical potential modulation of graphene. In-plane/out-of-plane SP-PW conversions are demonstrated with graphene ribbon/block-based meta-couplers. Converting SPs to single or two beams of PWs with variable radiation angles is realizable by varying the chemical potential of graphene without re-optimizing the structural parameters. © 2019 Optical Society of America

https://doi.org/10.1364/OL.44.003382

Surface plasmons (SPs) are evanescent waves bounded at a metal/dielectric interface, with the parallel wave vectors that are larger than the free-space value. Due to the unique characteristics of giant field enhancement at the nanoscale, SPs have found many applications in physics, chemistry, biology, and photonics [1]. To efficiently use SPs, a high-efficiency coupler is needed to convert the propagating waves (PWs) into SPs. However, the conventional coupling schemes, including prisms [2] and gratings [3], all suffer from low coupling efficiency or have bulky sizes, which is against the requirement of high-density optical integration on a chip.

Recently, it was shown that metasurfaces have provided an unprecedented approach to control over light waves [4–12]. Gradient metasurfaces provide an alternative method to compensate for the momentum mismatch between the PWs and SPs (or their counterparts, i.e., spoof SPs, at low frequency), and hence high-efficiency coupling between them is achievable [5,9]. Conversely, the SPs can be efficiently converted into directional PWs by properly arranging gradient-phase metasurfaces on the propagation path of SPs [7,13]. However, all these available SP-PW conversion meta-devices lack flexibility for active control.

Graphene, a monolayer of hexagonally arranged carbon atoms, has recently attracted special attention for its outstanding properties in developing active optoelectronic devices. Substantial progress on tunable free-space wave-front manipulation by using graphene metasurfaces, such as flat lenses and anomalous refraction of light, has been achieved [14–18]. While they have shown the capability of introducing interfacial phase gradient, and hence have great potential to compensate for the momentum mismatch between SPs and PWs, realizing dynamical conversion between the two types of electromagnetic (EM) waves still remains unexplored.

In this Letter, we propose to arrange graphene-based meta-couplers on the propagation path of a metal/dielectric/air (MDA) plasmonic waveguide to dynamically control SP-PW conversion. Here, graphene metasurfaces not only work as scattering sources but also provide an additional phase shift caused by plasmon resonance of graphene metasurfaces, resulting from plasmonic excitation. This thus allows one to dynamically tune the phase response of graphene metasurfaces by means of chemical potential modulation. Once the geometrical parameters of graphene metasurfaces are pre-designed, the phase shift between the emitted PWs and the SPs changes appreciably across a resonance by simply varying the chemical potential of graphene, μ_c. Consequently, a tunable phase gradient for emitted EM waves is achievable by chemical potential modulation of graphene without the requirement of re-optimizing the geometrical parameters. Two types of graphene-based meta-couplers are proposed to demonstrate dynamical in-plane and out-of-plane SP-PW conversions based on this design strategy. Moreover, the design flexibility for dynamical conversion can be further increased by using concepts of high-order metasurfaces. To the best of our knowledge, this is the first work on using graphene metasurfaces to realize dynamical SP-PW conversion. The resultant meta-coupler demonstrates its superiority over the conventional meta-coupler in terms of tunability, which does not allow dynamical SP-PW conversion [5,7,9,13].

Here, we consider SPs are excited on the left side and propagate toward graphene metasurfaces as shown in Fig. 1. The x component of the electric field of SPs can excite the plasmon resonance of each graphene ribbon/block with proper design of the structural parameters of a graphene metasurface. As a result,

the phase shift between the emitted EM waves and the SPs launched on the left side can be written as $\varphi^p + \varphi^s$, where φ^p and φ^s represent the phase shift accumulated by SP propagation and caused by plasmon resonance of graphene metasurfaces, respectively. Therefore, by spatially tailoring the geometry of a graphene ribbon/block metasurface in an array, the phase discontinuity can be well designed to reshape the wave fronts of the emitted PWs [Fig. 1]. Further, once the geometry is already designed, one can simply tune μ_c to dynamically modulate the phase discontinuity, so that a nearly arbitrary wave front of PWs is enabled. For graphene ribbon-based meta-couplers shown in Figs. 1(a) and 1(b), the phase shift can be varied along the x direction, so that SPs are purposely designed to convert into in-plane PWs, with the radiation angle being dynamically modulated by μ_c. Further, if graphene block metasurfaces are used, the phase shift can be independently designed along the x and y directions, and hence the SPs will be converted into out-of-plane PWs [Fig. 1(b)].

Now we will illustrate in detail how a graphene metasurface affects φ^p and φ^s. The metal/dielectric/graphene/air (MDGA) region and MDA region appear alternately along the propagation path of SPs [Fig. 1], and hence the influence of graphene on SP mode should be taken into account. First, we derive the modal eigenvalue equation of SP mode in MDGA by cooperating the Maxwell's equations with the boundary continuity conditions:

$$\varepsilon_d k_a \cos(k_d d) = i[k_d + k_a k_d \sigma_g/(\omega\varepsilon_0)]\sin(k_d d), \quad (1)$$

where $k_d = \sqrt{\varepsilon_d k_0^2 - \beta^2}$ and $k_a = \sqrt{k_0^2 - \beta^2}$, ε_d and ε_0 represent the relative permittivity of the dielectric and air, respectively, σ_g is the surface conductivity of graphene, k_0 and β denote the propagation constants of PWs in air ($k_0 = 2\pi/\lambda$, λ is fixed at 20 μm in this work) and SPs, respectively, and d is the thickness of the dielectric layer [Fig. 1]. In the simulation, graphene is characterized by its surface conductivity, related to Kubo formula, under the assumption of chemical potential, μ_c [19]:

$$\sigma_g = i\frac{e^2 k_B T}{\pi\hbar^2(\omega + i\tau^{-1})}\left[\frac{\mu_c}{k_B T} + 2\ln\left(\exp\left(-\frac{\mu_c}{k_B T}\right) + 1\right)\right] + i\frac{e^2}{4\pi\hbar}\ln\left[\frac{2|\mu_c| - \hbar(\omega + i\tau^{-1})}{2|\mu_c| + \hbar(\omega + i\tau^{-1})}\right], \quad (2)$$

where e is the electron charge, $\hbar$ is the reduced Planck's constant, ω is the radian frequency, and τ is the momentum relaxation time representing the loss mechanism. In our study, $T = 300$ K, $\tau = 0.64$ ps. The theoretical propagation constant extracted from Eq. (1) agrees well with the simulated results from the mode solution of *Lumerical* finite difference time domain (FDTD) [Fig. 2(a)]. It can be seen in Fig. 2(a) that β is slightly decreased from $1.19k_0$ to $1.16k_0$ as μ_c increases from 0.05 eV to 1 eV, resulting from increased surface conductivity of graphene. As shown in Fig. 2(b), the electrical field intensity distributions of SP mode for the MDA waveguide and MDGA waveguide with $\mu_c = 0.3$ eV or 0.8 eV are nearly the same. As a result, the phase shift accumulated by SP propagation at the graphene metasurface can be simply expressed as $\varphi^p = \beta L$, where L is the distance between the launched point of SPs and the graphene metasurface, and β is deemed as the average value of the propagation constant of the SP mode, i.e., $1.18k_0$, as μ_c ranges from 0.05 eV to 1 eV. We note in a recent study on graphene plasmons that the propagation of SPs was used to efficiently modulate the phase of SPs by changing μ_c [21]. However, in our case, it is an ineffective method of using φ^p to dynamically control the phase shift of the emitted EM waves since β is nearly unchangeable with μ_c. As for φ^s, the phase shift varies appreciably (nearly covers 0–2π range) across the resonance with either the chemical potential modulation of graphene or with the width variation of graphene [14–18], due to the interference effect between the plasmon resonance and Fabry–Perot resonance of building blocks in Figs. 1(a) and 1(b). As shown in Fig. 2(c), φ^s covers nearly full 2π range with the fixed geometry of graphene in Fig. 1(a), while μ_c varies from 0.05–1 eV. It is worth noting that, although realizing

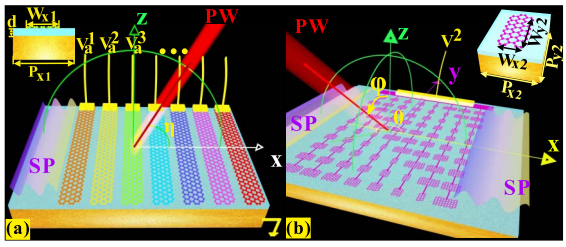

Fig. 1. (a) Schematic of graphene ribbon-based meta-coupler for dynamical in-plane SP-PW conversion. The inset on the left upper side is the unit cell, whose period along the x direction is P_{x1}. The width of the graphene ribbon along the x direction is denoted W_{x1}. η stands for the propagation angle, with respect to the positive x direction. The graphene metasurface has a length of Lx_1 along the x direction. (b) Schematic of graphene block-based meta-coupler for dynamical out-of-plane SP-PW conversion. The inset on the right upper side of (b) is the unit cell. All graphene blocks are imparted with one bias voltage by interconnecting them with graphene filaments along the y direction. P_{x2} and P_{y2} represent the periods of the unit cell along the x and y directions, respectively, and W_{x2} and W_{y2} denote the widths of the graphene blocks along the x and y directions, respectively. θ and φ represent the elevation and azimuth angle of the propagation direction, respectively. The graphene metasurface has an area of $Lx_2 \times Ly_2$. The thicknesses of the dielectric spacers are d.

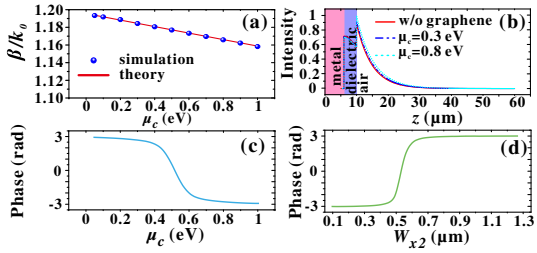

Fig. 2. (a) Propagation constant of SP mode in the MDGA waveguide versus μ_c. (b) Normalized electric field profiles of SP mode of the MDA waveguide and MDGA waveguide with $\mu_c = 0.3$ eV and 0.8 eV. (c) Reflection phase of the graphene ribbon versus μ_c. (d) Reflection phase of graphene block shown in Fig. 1(b) versus w_{x2}. Here, the refractive index of the dielectric layer is assumed to be 1.45, which is close to potassium bromide (KBr) at 20 μm [20]. Gold is selected as the metal layer with the relative permittivity of gold being described by a well-known Drude model as $\varepsilon = \varepsilon_\infty - f_p^2/(f_2 + if\gamma)$, where $f_p = 2069$ THz, $\gamma = 17.65$ THz, and $\varepsilon_\infty = 1.53$. In the simulation, W_{x1}, $P_{x1}(P_{x2})$, W_{y2}, and P_{y2} are set to 0.5 μm, 1 μm (1.5 μm), 0.2 μm, and 0.6 μm, respectively. d is fixed at 4 μm, and μ_c used in (d) is 0.8 eV.

μ_c from 0–1 eV might be difficult in experiment, the proposed graphene metasurface does not require such large variations of μ_c. In an experimental report on graphene, μ_c varying from 0.2–0.8 eV was achieved with electrostatic gating [22]. With μ_c being changed from 0.2 eV to 0.8 eV, here φ^s undergoes slight variation, as compared to that with μ_c from 0–1 eV, indicating the proposed graphene meta-coupler might be feasible in practical applications. In addition, as the mobility of graphene decreases, associated with the reduction of τ, the coverage of φ^s can be significantly modulated (not shown here). Our calculation results reveal that, φ^s can still cover nearly full 2π range as if τ reduces to 0.15 ps. The phase shift of the building block of the graphene block metasurface in Fig. 1(b) covers full 2π range with μ_c being fixed at 0.8 eV, while W_{x2} ranges from 0.1–1.3 μm [Fig. 2(d)]. To briefly conclude here, it is rather robust and flexible to dynamically control the phase shift of the emitted EM waves by using plasmon resonance of graphene metasurfaces [presented in Figs. 1(a) and 1(b)] with either chemical potential modulation or geometry design.

Now, we will consider how to use the graphene ribbon-based meta-coupler to convert the SPs to in-plane PWs. It is assumed that 400 units of graphene ribbons are arranged along the propagation path of SPs [Fig. 1(a)], associated with $Lx_1 = 400$ μm. The phase shift of the emitted EM waves at the mth unit ($m \in [1, 400]$) can be written as $\varphi^p_m + \varphi^s_m$, where $\varphi^p_m = \beta(m-1)P_{x1}$ and φ^s_m denote the phase shift at the mth unit. $\varphi^p_m = \beta(m-1)P_{x1}$ is the phase shift accumulated by SP propagation, with respect to the SPs at the first unit, and φ^s_m is the phase shift caused by plasmon resonance of mth graphene ribbon. The far-field function of PWs from all the scattered SPs can be expressed as [23]

$$f(\eta) = \sum_{m=1}^{M} \exp(-\alpha m P_{x1}) \cdot \exp\{i[\varphi^s_m + \beta(m-1)P_{x1} + k_0(m-1)P_{x1}\cos\eta]\}, \quad (3)$$

where α represents the total loss cofficient from SP scattering and propagation. In order to diffract the SPs into a specific direction, the scattered SPs by each graphene ribbon should be in phase, yielding the following condition:

$$d\varphi^s/dx + \beta - k_x = 0, \quad (4)$$

where $k_x = k_0 \cos\eta$ represents the transverse wave vector of the emitted PWs, and $d\varphi^s/dx$ is the phase gradient of the graphene metasurface. This equation is equivalent to the transverse wave-vector matching condition [7].

Here, three graphene metasurfaces C1, C2, and C3 are designed with different phase gradients of $2\pi/40$ rad/μm, $2\times 2\pi/40$ rad/μm, and $3\times 2\pi/40$ rad/μm, respectively, without changing the geometry, and the phase distributions of φ^s within a supercell are shown in Fig. 3(a). Metasurface C1 is a normal gradient metasurface with a supercell period of 40 μm and the phase distributions within a supercell are shown in Fig. 3(a). By choosing the chemical potential for each graphene ribbon [Fig. 3(b)], the linear phase distributions within a supercell can be obtained. As for C2 and C3, the concept of high-order metasurfaces is introduced to realize the required phase gradients [Fig. 3(a)] [16,18]. C2 (C3) shares the same supercell with C1, but selects every other (three) μ_c from C1 [Fig. 3(b)]. The phase coverage within a supercell and phase gradient for C2 (C3) thus become $2\times 2\pi$ ($3\times 2\pi$) and $2\times 2\pi/40$ rad/μm ($3\times 2\pi/40$ rad/μm), respectively [Fig. 3(a)]. According to Eq. (4), C1, C2, and C3 are highly expected to convert SPs into PWs with the propagation angles of 47°, 80°, and 109°, respectively. The simulation results in Fig. 3(c) show that the SPs are converted into PWs with the propagation angles of 45°, 77°, and 106° for C1, C2, and C3, respectively, nearly the same as those predicted by Eq. (4). Further, we employed Eq. (3) and FDTD simulation to retrieve the far-field profile of $|E|^2$ versus the spatial angle for the PWs [Fig. 3(d)]. The theoretically estimated far-field diffraction patterns extracted with Eq. (3) by using $\alpha = 0.02$ (1/μm) agree well with the simulated results.

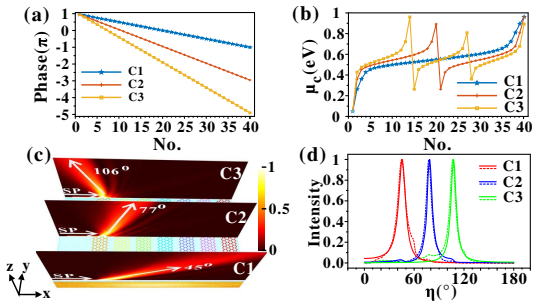

Fig. 3. (a), (b) Reflection phase shift (a) and μ_c (b) of each graphene ribbon within a supercell of C1, C2, and C3. (c) Simulated near-field distributions of electric field intensity in the x-z plane for C1–C3. (d) Theoretically estimated (solid lines) and simulated (dashed lines) normalized far-field patterns of electric field intensity for C1–C3.

To realize out-of-plane SP-PW conversion, it is assumed that the graphene block metasurfaces consist of 135 × 360 units of graphene blocks, associated with a total area of 202.5 μm(Lx_2) × 216 μm(Ly_2). In this case, one can properly set W_{x2} for each graphene block to independently control the phase shifts along the x and y directions, caused by plasmon resonance of graphene block metasurfaces. When SPs propagate toward the graphene blocks along the x direction, the far-field function of PWs from all the scattered SPs of graphene block metasurfaces can be rewritten as [23]

$$f(\theta,\varphi) = \sum_{n=1}^{N}\sum_{m=1}^{M} \exp(-\alpha m P_{x2}) \cdot \exp\{i[\varphi^s_{mn} + \beta(m-1)P_{x2} - k_x(m-1)P_{x2} - k_y(n-1)P_{y2}]\}, \quad (5)$$

where φ^s_{mn} represents the phase shift caused by plasmon resonance with the (mth, nth) graphene block, M, N denote the total number of graphene blocks along the x and y directions, respectively, k_x and k_y are the transverse wave vector of PWs along the x and y directions, respectively. Similarly, the transverse wave vector of PWs along the x and y directions can be expressed as

$$\begin{cases} k_x = k_0 \sin\theta\cos\varphi = \partial\varphi^s/\partial x + \beta \\ k_y = k_0 \sin\theta\sin\varphi = \partial\varphi^s/\partial y \end{cases}, \quad (6)$$

where $\partial\varphi^s/\partial x$ and $\partial\varphi^s/\partial y$ represent the phase gradients of graphene metasurfaces along the x and y directions, respectively.

By appropriately choosing W_{x2} for each graphene block (W_{y2} is fixed at 0.2 μm), one is able to introduce different phase gradients along the x and y directions with $\mu_c = 0.8$ eV. The W_{x2} versus the coordinates (x, y) is described in Fig. 4(a), with W_{x2} span from 0.1–1.3 μm. The phase shift, φ^s, caused

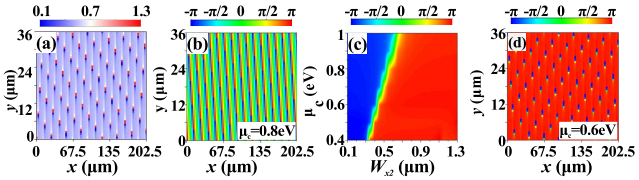

Fig. 4. (a) Designed W_{x2} (μm) versus the coordinates (x, y). (b) Scattered phase shift, φ^s, versus the coordinates (x, y) with $\mu_c = 0.8$ eV. (c) Scattered phase shift, φ^s, versus W_{x2} and μ_c. (d) Scattered phase shift, φ^s, versus the coordinates (x, y) as μ_c is 0.6 eV. We have merely plotted 1/6 of graphene block area along the y direction (216 μm), since the lattice constant of a supercell along the y direction is 36 μm. In the simulations, all the other geometrical parameters are the same as those in Fig. 2(d).

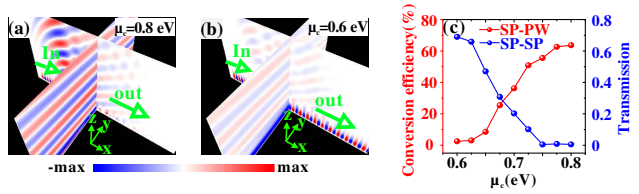

Fig. 5. (a), (b) Simulated near-field distributions of the z component of electric field intensity in the x-z and y-z planes, when μ_c is set to be 0.8 and 0.6 eV, respectively. (c) SP-PW conversion efficiency (red line) and intensity transmission of SPs (blue line) as a function of μ_c.

by plasmon resonance, versus the coordinates (x, y) is depicted in Fig. 4(b), which clearly indicates that both linear phase gradients along the x and y directions are provided. The phase gradients along the x and y directions are $-1.5k_0$ and $-0.5k_0$, respectively. The elevation and azimuth angles of the propagation direction of PWs estimated by Eq. (6) are $\theta = 40°$ and $\varphi = 240°$, respectively. The simulated near-field distributions of E_z also validate that the SPs are efficiently converted to an out-of plane PW [Fig. 5(a)]. When μ_c is tuned down so that the working frequency is gradually far away from the resonance frequency [Fig. 4(c)], φ^s versus the coordinates (x, y) is varied accordingly, and the radiation strength of graphene metasurfaces is weakened. As shown in Fig. 4(d), the phase shifts of the metasurface are no longer linearly distributed with 0.6 eV, despite the full phase coverage from $-\pi$ to π. As a result, when μ_c is fixed at 0.6 eV, most of the SPs are directly transmitted through the metasurface, and the intensity of the PW is weakened [Fig. 5(b)]. To further confirm the effect of μ_c on SP-PW conversion efficiency, the SP-PW conversion efficiency versus the μ_c is calculated. As shown in Fig. 5(c), the transmission efficiency of SPs is enhanced from 0% to 68%, with SP-PW conversion efficiency being decreased from 63% to 2.5%.

In summary, we have proposed to employ graphene-based meta-couplers to dynamically control SP-PW conversion by means of chemical potential modulation of graphene to provide a tunable phase shift to the scattering SPs from graphene metasurfaces. Graphene ribbon/block-based meta-couplers present the capability of realizing in-plane/out-of-plane SP-PW conversions. We have theoretically and numerically demonstrated that SPs can be converted into PWs with variable propagation directions by varying the chemical potential of graphene without re-optimizing the structural parameters. The concepts of high-order metasurfaces can be readily used for the design, and hence provide extra freedom to diversified control of SP-PW conversion. These results pave a promising avenue to realization of dynamical SP-PW conversion and can stimulate contructing dynamical optical devices linking SPs and PWs.

Funding. National Natural Science Foundation of China (NSFC) (11474116, 11674118, 11774186).

REFERENCES

1. W. L. Barnes, A. Dereux, and T. W. Ebbesen, Nature **424**, 824 (2003).
2. A. Otto, Z. Phys. **216**, 398 (1968).
3. Y. Tang, Z. Wang, L. Wosinski, U. Westergren, and S. He, Opt. Lett. **35**, 1290 (2010).
4. N. Yu, P. Genevet, M. A. Kats, F. Aieta, J.-P. Tetienne, F. Capasso, and Z. Gaburro, Science **334**, 333 (2011).
5. S. Sun, Q. He, S. Xiao, Q. Xu, X. Li, and L. Zhou, Nat. Mater. **11**, 426 (2012).
6. M. Decker, I. Staude, M. Falkner, J. Dominguez, D. N. Neshev, I. Brener, T. Pertsch, and Y. S. Kivshar, Adv. Opt. Mater. **3**, 813 (2015).
7. J. J. Xu, H. C. Zhang, Q. Zhang, and T. J. Cui, Appl. Phys. Lett. **106**, 021102 (2015).
8. W. T. Chen, A. Y. Zhu, V. Sanjeev, M. Khorasaninejad, Z. Shi, E. Lee, and F. Capasso, Nat. Nanotechnol. **13**, 220 (2018).
9. F. Ding, R. Deshpande, and S. I. Bozhevolnyi, Light Sci. Appl. **7**, 17178 (2018).
10. S. Wang, P. C. Wu, V.-C. Su, Y.-C. Lai, M.-K. Chen, H. Y. Kuo, B. H. Chen, Y. H. Chen, T.-T. Huang, and J.-H. Wang, Nat. Nanotechnol. **13**, 227 (2018).
11. T. Yang, H. Lin, and B. Jia, Front. Optoelectron. **11**, 2 (2018).
12. X. Kong, J. Xu, J.-J. Mo, and S. Liu, Front. Optoelectron. **10**, 124 (2017).
13. H. Zhu, T. Xu, Z. Wang, J. Li, Z. Hang, L. Zhou, S. Chen, X. Li, and L. Chen, Opt. Express **26**, 28531 (2018).
14. T. Yatooshi, A. Ishikawa, and K. Tsuruta, Appl. Phys. Lett. **107**, 053105 (2015).
15. W. Ma, Z. Huang, X. Bai, P. Zhan, and Y. Liu, ACS Photon. **4**, 1770 (2017).
16. C. Wang, W. Liu, Z. Li, H. Cheng, Z. Li, S. Chen, and J. Tian, Adv. Opt. Mater. **6**, 1701047 (2018).
17. E. Carrasco, M. Tamagnone, and J. Perruisseau-Carrier, Appl. Phys. Lett. **102**, 104103 (2013).
18. Z. Li, J. Hao, L. Huang, H. Li, H. Xu, Y. Sun, and N. Dai, Opt. Express **24**, 8788 (2016).
19. V. P. Gusynin, S. G. Sharapov, and J. P. Carbotte, J. Phys. Condens. Matter **19**, 026222 (2007).
20. E. D. Palik, *Handbook of Optical Constants of Solids* (Academic, 1991), Vol. **2**.
21. A. Woessner, Y. Gao, I. Torre, M. B. Lundeberg, C. Tan, K. Watanabe, T. Taniguchi, R. Hillenbrand, J. Hone, M. Polini, and F. H. L. Koppens, Nat. Photonics **11**, 421 (2017).
22. Z. Fang, Y. Wang, A. E. Schlather, Z. Liu, P. Ajayan, F. J. García de Abajo, P. Nordlander, X. Zhu, and N. Halas, Nano Lett. **14**, 299 (2014).
23. T. J. Cui, M. Q. Qi, X. Wan, J. Zhao, and Q. Cheng, Light Sci. Appl. **3**, e218 (2014).